AIAA JOURNAL
Vol. 39, No. 10, October 2001

Sound from Turbulence Convected by a Parallel Flow Within a Rectangular Duct

S. J. Leib*
Ohio Aerospace Institute, Brookpark, Ohio 44142
and
M. E. Goldstein†
NASA John H. Glenn Research Center at Lewis Field, Cleveland, Ohio 44135

A previously derived high-frequency solution to Lilley's equation is used to study the far-field characteristics of the sound generated by a turbulent flow within a semi-infinite duct of nonaxisymmetric cross section. The source term is simplified by assuming the turbulence to be axisymmetric about the mean flow direction, and a relatively simple formula for the far-field azimuthal and polar sound field variation is obtained. The numerical computations involve the calculation of ray trajectories, and a parallel computer code has been developed for this purpose. It is expected that the code will be able to produce azimuthal directivity patterns in a few minutes on a large parallel computer system. The method has been applied to a rectangular duct, and numerical results for the azimuthal and polar variation of the sound field were computed on a cluster of workstations for a number of duct aspect ratios, wall impedances values, and source locations.

Nomenclature

A	=	duct aspect ratio
a, b	=	mean Mach number profile parameters
$\bar{c}$	=	mean speed of sound
$\boldsymbol{f}$	=	fluctuating force per unit volume
I	=	acoustic spectral density
i	=	$\sqrt{-1}$
k	=	acoustic wave number
$\mathcal{L}$	=	differential operator for Lilley equation
M	=	mean Mach number
n	=	mean Mach number profile parameter
p	=	normalized acoustic pressure fluctuation
R	=	distance between source and observation points
R_{ij}	=	second-order, two-point, time-delayed correlation function
R_{ijkl}	=	fourth-order, two-point, time-delayed correlation function
$\mathcal{R}_i$	=	reflection coefficient
r	=	superellipse parameter
S	=	Eikenal
t	=	time
U	=	mean streamwise velocity
u_i	=	fluctuating velocity in the x_i direction
$\boldsymbol{x}$	=	Cartesian coordinate vector
Γ	=	acoustic source distribution
γ	=	ray speed
δ	=	Dirac delta function
ζ	=	normalized wall impedance
θ	=	polar angle measured from jet axis
λ, μ	=	initial ray angles
$\boldsymbol{\xi}$	=	separation vector
ρ	=	density
τ	=	time delay
ϕ	=	azimuthal angle
χ	=	duct cross-sectional function
ω	=	angular frequency

Subscripts

c	=	convection
G	=	Green's function
s	=	source
1	=	streamwise direction
2, 3	=	transverse directions
∞	=	ambient
$-$	=	quantity incident on wall

Superscript

s	=	source

Introduction

THE use of mixer–ejector nozzles to reduce jet noise has focused attention on the problem of predicting the sound field generated by sources located within the nozzle. Whereas mixer-ejector nozzles are capable of significantly reducing the overall mixing noise, they also introduce new sources of high-frequency noise within the ejector. Overall sound reduction is achieved by using acoustic liners on the ejector walls to absorb as much of the internally generated sound as possible.

The externally generated noise tends to be fairly axisymmetric, presumably because the dominant sound sources lie at the end of the potential core where the flowfield itself is axisymmetric. However, the internal flow can be highly nonaxisymmetric, and the internally generated noise is likely to have significant azimuthal variation. It would, therefore, be very useful to have a theoretically based scheme for calculating the far-field characteristics of the internally generated noise for various nozzle shapes and flow conditions.

Goldstein and Rosenbaum[1] used Lighthill's equation to develop a general theory for predicting the sound radiated by a turbulent flow in the presence of solid boundaries. Dill et al.[2] extended this analysis to account for mean-flow refraction effects. However, both theories involve the solution of a complicated Weiner–Hopf problem, whose solution can only be explicitly worked out for a plug flow mean velocity profile. Because the internally generated noise appears to be of much higher frequency than that generated externally, it seems appropriate to use a high-frequency approximation to simplify and extend these previous analyses of this problem.

Goldstein[3] developed a high-frequency solution for the sound radiation from a convecting point-quadrupole source in an arbitrary, transversely sheared mean flow. This solution was later extended by Durbin[4] to account for a general (not necessarily parallel) mean flow. Both of these solutions involve a ray-spreading factor that multiplies

Received 7 November 2000; presented as Paper 2001-0818 at the AIAA 39th Aerospace Sciences Meeting, Reno, NV, 8–11 January 2001; revision received 1 May 2001; accepted for publication 2 May 2001. This material is declared a work of the U.S. Government and is not subject to copyright protection in the United States.

*Senior Research Associate, Institute for Computational Mechanics in Propulsion. Senior Member AIAA.
†Chief Scientist. Fellow AIAA.

the product of a source function, which describes the actual acoustic sources, with some Doppler factors that account for the local source and mean-flow convection effects. The spreading factor accounts for the mean-flow variation along the path of the radiated sound and can be calculated from geometric acoustics, or ray tracing. The ray tracing can be reduced to a two-dimensional problem[3] when the mean flow is parallel, which greatly simplifies the computation.

Goldstein and Leib[5] showed that the formula derived in Ref. 3 still applies to the internally generated noise and that only the ray-tracing analysis, which is used to calculate the ray-spreading factor, needs to be modified to account for the effect of the nozzle walls. However, the ray-tracing computation remains two dimensional. Sample numerical results were presented in Ref. 5 for the special case of a ring source in a circular duct with an axisymmetric mean flow.

The amount of computation increases substantially when the geometry is nonaxisymmetric because many more ray trajectories must be computed to determine the azimuthal and polar characteristics of the far-field sound. However, each ray trajectory is completely independent of all of the others and only involves the solution of a small system of ordinary differential equations. The calculations are, therefore, ideally suited to parallel processing techniques.

This paper describes a study of the far-field characteristics of the sound generated within a nonaxisymmetric nozzle using the solution derived in Ref. 5, and the development of a computer code for the parallel computation of the required ray trajectories.

An application of geometric acoustics to the computation of high-frequency engine-intake noise was initiated by Kempton.[6] In the absence of mean flow, it was shown that the simple ray theory predictions of the far-field sound compared well with those obtained using a more conventional modal-type analysis. The ray acoustics approach has the advantage of being able to handle ducts of arbitrary cross section containing an arbitrary mean flow in a straightforward way.

A rectangular mixer was the nozzle of choice for the recently canceled high-speed transport and is the logical choice for the next generation of high-speed aircraft. The present computations are, therefore, restricted to this configuration. Results are presented for the azimuthal and polar variation of the sound field as a function of duct aspect ratio, source distribution, and wall impedance.

Formulation and Review of the High-Frequency Solution

We consider a unidirectional, transversely sheared, parallel mean flow exiting from a parallel-walled nozzle, within which lies a distribution of acoustics sources. The mean velocity is assumed to go smoothly to zero at the generators of the nozzle walls and to remain zero beyond that surface. The configuration is shown in Fig. 1. For an ideal gas, the propagation of small-amplitude acoustic disturbances on such a mean flow is governed by[7]

$$\mathcal{L}p \equiv \frac{\mathrm{D}}{\mathrm{D}t}\left(\frac{\mathrm{D}^2 p}{\mathrm{D}t^2} - \nabla\cdot\bar{c}^2\nabla p\right) + 2\bar{c}^2\nabla U\cdot\nabla\frac{\partial p}{\partial x_1} = \Gamma \quad (1)$$

where p denotes the acoustic pressure fluctuation normalized by $\bar{\rho}\bar{c}^2$, with $\bar{\rho}$, $\bar{c}$, and U being the mean density, sound speed, and velocity, respectively, which are functions of the transverse coordinate vector $\boldsymbol{x}_t = \{x_2, x_3\}$,

$$\frac{\mathrm{D}}{\mathrm{D}t} \equiv \frac{\partial}{\partial t} + U\frac{\partial}{\partial x_1} \quad (2)$$

is the convective derivative, t is the time, and x_1 is the Cartesian coordinate in the streamwise direction.

Γ represents the acoustic source distribution, which is related to the fluctuating force f_i per unit volume by

$$\Gamma = \frac{\mathrm{D}}{\mathrm{D}t}\nabla\cdot\boldsymbol{f} - 2\nabla U\cdot\frac{\partial \boldsymbol{f}}{\partial x_1} \quad (3)$$

In the absence of temperature fluctuations, Lilley's equation is obtained by replacing f_i by the quadrupole source distribution $f_i = \partial u_i u_j/\partial x_j$, where u_i is the velocity fluctuation within the flow.

Green's Function

Because the problem is linear, and because the second term in Eq. (3) is negligible compared to the first in the high-frequency limit, the solution for an arbitrary force distribution f_i can be obtained by superposition of solutions, for example, p_G, to

$$\mathcal{L}\left(p_G e^{-i\omega t}\right) = \frac{\mathrm{D}}{\mathrm{D}t}\delta(\boldsymbol{x}-\boldsymbol{x}^s)e^{-i\omega t} \quad (4)$$

where $\boldsymbol{x}^s$ is the source position.

The solution to this problem is given by[3–5]

$$p_G = p_G(\boldsymbol{x}\,|\,\boldsymbol{x}^s,\omega) = (1-Ms_1)\bar{\mathcal{R}}\Phi e^{ikS} \quad (5)$$

in the high-frequency limit

$$k \equiv \omega/\bar{c}_\infty \to \infty \quad (6)$$

where $\bar{c}_\infty$ is the speed of sound in the region of zero mean flow,

$$M \equiv U/\bar{c}_\infty \quad (7)$$

is the mean Mach number, and S is the Eikenal, which satisfies the Eikenal equation

$$(1-Ms_1)^2 - (\bar{c}/\bar{c}_\infty)^2|\boldsymbol{s}|^2 = 0 \quad (8)$$

where

$$\boldsymbol{s} = \{s_1, s_2, s_3\} \equiv \nabla S \quad (9)$$

The solution to this first-order partial differential equation can be obtained by the method of characteristics by calculating S along the ray trajectories $\boldsymbol{x}(\tau)$, which are determined by the ordinary differential equations

$$\dot{s}_1 = 0 \quad (10)$$

$$\dot{x}_1 = s_1\left[1 - \left(\frac{U}{\bar{c}}\right)^2\right] + \frac{U\bar{c}_\infty}{\bar{c}^2} \quad (11)$$

$$\dot{x}_i = s_i, \qquad \dot{s}_i = \frac{1}{2}\frac{\partial}{\partial x_i}\left(\frac{s_1 U - \bar{c}_\infty}{\bar{c}}\right)^2, \qquad i = 2, 3 \quad (12)$$

subject to the initial conditions at the source position $\boldsymbol{x}^s$ that the initial ray velocity is proportional to the initial ray direction, $\{\cos\mu, \sin\mu\cos\lambda, \sin\mu\sin\lambda\}$, that is, that

$$\dot{\boldsymbol{x}}_s = \gamma_s\{\cos\mu, \sin\mu\cos\lambda, \sin\mu\sin\lambda\} \quad (13)$$

where τ is a parameter that varies continuously along the ray, the dot denotes differentiation with respect to τ, the subscript s denotes quantities evaluated at the source position $\boldsymbol{x}^s$, and the proportionality constant γ_s is given by[5]

$$\gamma_s^{-2} = (\bar{c}_s/\bar{c}_\infty)^2\left\{1 - [(U_s/\bar{c}_s)\sin\mu]^2\right\} \quad (14)$$

The reflection coefficient $\bar{\mathcal{R}}$ is given by

$$\bar{\mathcal{R}} \equiv \prod_{i=1}^{m}\mathcal{R}_i \quad (15)$$

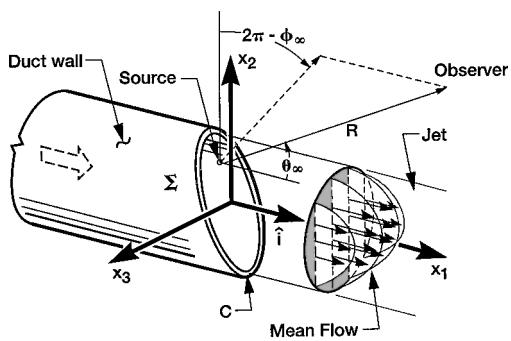

Fig. 1 Flow configuration.

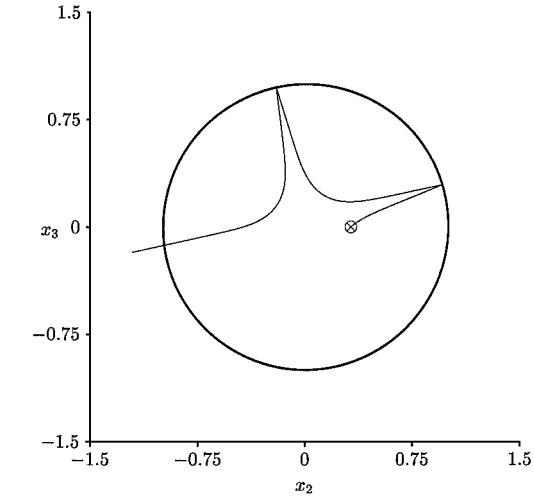

a) Transverse plane

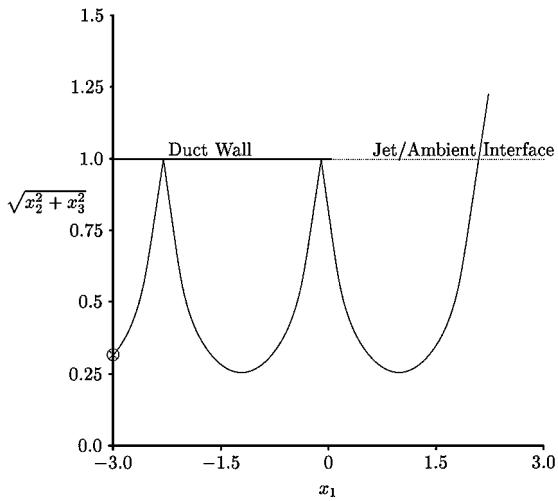

b) Streamwise-radial plane

Fig. 2 Projections of a typical ray trajectory emanating from a source location (marked by ⊗) inside a circular duct.

where $\mathcal{R}_i$ denotes the ith individual reflection coefficient, which (upon dropping the subscript i) is given by

$$\mathcal{R} = (\eta + 1)/(\eta - 1) \tag{16}$$

where

$$\eta \equiv -(\boldsymbol{s}_- \cdot \hat{\boldsymbol{n}})\zeta \tag{17}$$

the minus subscript on $\boldsymbol{s}$ refers to the ray incident on the wall whose outward unit normal is $\hat{\boldsymbol{n}}$, and ζ is the normalized wall impedance, for each of the m reflections that the ray undergoes before leaving the duct.

An example of a typical ray trajectory emanating from a source location within the duct is shown in Fig. 2 for the case of a circular duct. The rays of interest propagate downstream (Fig. 2b) as they are refracted by the mean flow, reflecting (possibly multiple times) off the duct walls before leaving the duct and arriving at an observer location in the far field.

In the acoustic far field, the rays are again straight lines and are given by

$$\boldsymbol{x} = \boldsymbol{x}^s + R(\cos\theta_\infty, \sin\theta_\infty \cos\phi_\infty, \sin\theta_\infty \sin\phi_\infty) \tag{18}$$

where R can be taken as the distance between the source point and the observation point and θ_∞ and ϕ_∞ are the far-field polar and circumferential angles, respectively (see Fig. 1). The amplitude function Φ is then given by

$$\Phi \to \frac{1}{4\pi R \bar{c}_\infty^2 (1 - M_s \cos\theta_\infty)} \sqrt{\left|\frac{\mathrm{d}\lambda}{\mathrm{d}\phi_\infty}\right|} \tag{19}$$

Also,

$$s_1 = \cos\theta_\infty \tag{20}$$

$$S = \left(x_1 - x_1^s\right)\cos\theta_\infty + S_0\left(\boldsymbol{x}_t \,|\, \boldsymbol{x}_t^s\right) \tag{21}$$

The far-field polar angle θ_∞ reached by rays emanating from a given source location depends only on the initial polar angle μ and not on λ (Ref. 5), so that the former can be eliminated from the initial condition (13) and explicit solutions can be obtained directly for a specified θ_∞. This is equivalent to reducing the computation to a two-dimensional ray-tracing problem and results in considerable computational savings.

Application to Sound Radiated by a Turbulent Flow

By assuming source compactness, far-field Green's function (5) and (19) can be used to calculate the acoustic spectral density, defined as the Fourier transform of the autocorrelation of the normalized acoustic pressure, due to a unit volume of turbulence at $\boldsymbol{x}^s$. The result is[5,8,9]

$$I\left(\boldsymbol{x}, \boldsymbol{x}^s \,|\, \omega_s\right) = \frac{k_s^4 \Psi_{ijkl} D_{ijkl}}{[4\pi R \bar{c}_s \bar{c}_\infty (1 - M_s \cos\theta_\infty)]^2} \tag{22}$$

where $k_s = \omega_s / \bar{c}_s$ and

$$\omega_s = (1 - M_c \cos\theta_\infty)\omega \tag{23}$$

is the source frequency. The spectral source strength Ψ_{ijkl} is related to the fourth-order, two-point, time-delayed correlation function of the turbulence

$$R_{ijkl}(\boldsymbol{x}^s, \boldsymbol{\xi}, \tau) = \overline{u_i' u_j' u_k'' u_l''} - \overline{u_i' u_j'}\,\overline{u_k'' u_l''} \tag{24}$$

by

$$\Psi_{ijkl} = \int_{-\infty}^{\infty} \int e^{i\omega_s \tau} R_{ijkl}(\boldsymbol{x}^s, \boldsymbol{\xi}, \tau)\, \mathrm{d}\boldsymbol{\xi}\, \mathrm{d}\tau \tag{25}$$

where the single prime indicates that the quantity is evaluated at the position and time $(\boldsymbol{x}^{s'}, t)$, the double prime indicates the position and time $(\boldsymbol{x}^{s''}, t + \tau)$,

$$\boldsymbol{\xi} = \boldsymbol{x}^{s''} - \boldsymbol{x}^{s'} - \hat{\boldsymbol{i}} U_c \tau \tag{26}$$

and

$$\boldsymbol{x}^s = \left\{x_1^{s'}, \tfrac{1}{2}\left(x_2^{s'} + x_2^{s''}\right), \tfrac{1}{2}\left(x_3^{s'} + x_3^{s''}\right)\right\} \tag{27}$$

is the mean position of the source.

When the asymptotically small ray-interference effects are neglected,[5]

$$D_{ijkl} = \sum_{n=1}^{\kappa} \sigma_i^{(n)} \sigma_j^{(n)} \sigma_k^{(n)} \sigma_l^{(n)} \left|\bar{\mathcal{R}}^{(n)}\right|^2 \left|\frac{\partial \lambda^{(n)}}{\partial \phi_\infty}\right| \tag{28}$$

where the sum is taken over all rays reaching the observer and

$$\sigma_1^{(n)} = \frac{\cos\theta_\infty}{1 - M_c \cos\theta_\infty} \tag{29}$$

$$\sigma_2^{(n)} = \frac{q_s \cos\lambda^{(n)}}{1 - M_c \cos\theta_\infty}, \qquad \sigma_3^{(n)} = \frac{q_s \sin\lambda^{(n)}}{1 - M_c \cos\theta_\infty} \tag{30}$$

where

$$q_s = \sqrt{\frac{(1 - M_s \cos\theta_\infty)^2}{(\bar{c}_s / \bar{c}_\infty)^2} - \cos^2\theta_\infty} \tag{31}$$

The sum in Eq. (28) includes contributions from rays reaching the observation point directly from the source location as well as any that arrive there after reflecting off the duct walls and off of any caustics that may appear in the flow. Although the geometric acoustics solution is not actually valid at a caustic itself, the ray equations may be integrated through the caustic to obtain the solution in the much larger external region. Because the caustic only affects the external

solution by introducing a constant phase shift,[3] the solution (22), with Eq. (28), which neglects these phase changes,[5] is valid everywhere outside the zone of silence and the asymptotically negligible regions surrounding the caustics, to the order of approximation considered here.

Durbin[10] showed that nonparallel flow effects eliminate the strict zone of silence and that instead the sound field becomes rapidly, but continuously, small as the jet axis is approached. Weak nonparallel mean-flow effects could be incorporated into the present analysis and computations by allowing the mean Mach number and sound speed to depend parametrically on the streamwise coordinate. This quasi-parallel approximation represents an intermediate approach between the completely parallel flow case considered here and the fully nonparallel case, which would require a much more time-consuming, three-dimensional ray-tracing computation.[4] Because we have not attempted to include nonparallel mean-flow effects at any level in this paper, the numerical results will be restricted to polar angles outside the zone of silence.

It is usual to make a number of assumptions about the turbulence to simplify the form of the source function in Eq. (22). Here we will assume that the turbulence is quasi normal and axisymmetric about the mean-flow direction. Then R_{ijkl} can be expressed as the product of second-order correlations,[11,12]

$$R_{ijkl} = R_{ik}R_{jl} + R_{il}R_{jk} \tag{32}$$

$$\begin{aligned}\sigma_i^{(n)}\sigma_j^{(n)}\sigma_k^{(n)}\sigma_l^{(n)}\Psi_{ijkl} = 2\Bigg\{&\left|\boldsymbol{\sigma}^{(n)}\right|^4 \int_{-\infty}^{\infty}\int e^{i\omega_s\tau}\bar{Q}_0\,\mathrm{d}\xi\,\mathrm{d}\tau \\ &- 2\left(\sigma_2^{(n)}\sigma_3^{(n)}\right)^2 \int_{-\infty}^{\infty}\int e^{i\omega_s\tau}(\bar{Q}_{23}-\bar{Q}_{22})\,\mathrm{d}\xi\,\mathrm{d}\tau \\ &+ \sigma_i^{(n)^2}\sigma_j^{(n)^2}\int_{-\infty}^{\infty}\int e^{i\omega_s\tau}\bar{Q}_{ij}\,\mathrm{d}\xi\,\mathrm{d}\tau\Bigg\}\end{aligned} \tag{33}$$

where

$$\begin{aligned}&\bar{Q}_{11} = R_{11}^2 - R_{12}^2, \qquad \bar{Q}_{12} = \bar{Q}_{13} = R_{12}^2 + R_{11}R_{22} \\ &\bar{Q}_{22} = \bar{Q}_{33} = R_{22}^2 - R_{12}^2, \qquad \bar{Q}_{23} = R_{22}^2 - R_{23}^2, \qquad \bar{Q}_0 = R_{12}^2\end{aligned} \tag{34}$$

are symmetric in their indices.[1,9]

Mean-Flow and Source Distribution Models

We introduce an orthogonal coordinate system (χ, φ), where

$$\chi(x_2, x_3) = 1, \qquad x_1 < 0 \tag{35}$$

describes the surface of the duct, and

$$\nabla\chi(x_2, x_3)\cdot\nabla\varphi(x_2, x_3) = 0 \tag{36}$$

and assume that the mean Mach number and sound speed profiles only depend on χ. We also model the source distribution, which in reality is the whole of the turbulent flow, as a generalized "ring" residing within the duct, that is,

$$\chi\left(x_2^s, x_3^s\right) \equiv \chi_s = \text{const}, \qquad x_1 = x_1^s < 0 \tag{37}$$

Integrating Eq. (22) over the model source distribution and assuming that the turbulence statistical quantities are constant along $\chi = \chi_s$, yields

$$\begin{aligned}I(\boldsymbol{x}\mid\omega_s) = &\frac{k_s^4}{2\left[2\pi R\bar{c}_s\bar{c}_\infty(1-M_s\cos\theta_\infty)(1-M_c\cos\theta_\infty)^2\right]^2} \\ &\times\left\{\frac{[1-M_s\cos\theta_\infty]^4}{(\bar{c}_s/\bar{c}_\infty)^4}\mathcal{Q}_0 + \cos^4\theta_\infty\mathcal{Q}_{11}\right. \\ &\left. + 2q_s^2\cos^2\theta_\infty\mathcal{Q}_{12} + q_s^4\mathcal{Q}_{22}\right\}\mathcal{I}_1\end{aligned} \tag{38}$$

where

$$\mathcal{Q}_\alpha = \int_{-\infty}^{\infty}\int e^{i\omega_s\tau}\bar{Q}_\alpha\,\mathrm{d}\xi\,\mathrm{d}\tau \tag{39}$$

$$\mathcal{I}_1 = \int\sum_{n=1}^{\kappa}\left|\bar{\mathcal{R}}^{(n)}\right|^2\left|\frac{\partial\lambda^{(n)}}{\partial\phi_\infty}\right|\mathrm{d}l \tag{40}$$

where $\mathrm{d}l$ is an element of arc length along the source and the range of integration in Eq. (40) is the entire source distribution.

Equations (38–40) show that the far-field azimuthal directivity is completely determined by the factor $\mathcal{I}_1$, which implies that the azimuthal directivity at a fixed far-field polar angle is independent of the axisymmetric turbulence model, as well as the degree of anisotropy. It is, however, influenced by the effects of ray propagation through the mean flow via the ray-spreading factor and, in the case of a soft-wall duct, also by the reflection coefficient. However, the polar variation does depend on the turbulence characteristics as well as on ray-propagation effects.

The azimuthally averaged polar directivity,

$$\bar{I} \equiv \frac{1}{2\pi}\int_{-\pi}^{\pi} I(\boldsymbol{x}\mid\omega_s)\,\mathrm{d}\phi_\infty \tag{41}$$

is also of interest.

Substituting Eq. (38) with Eqs. (39) and (40) into Eq. (41), interchanging the order of integration, and changing integration variables shows that $\bar{I}$ is given by the same expression as $I(\boldsymbol{x}\mid\omega_s)$, but with $\mathcal{I}_1$ replaced by

$$\bar{\mathcal{I}}_1 = \frac{1}{2\pi}\iint\left|\bar{\mathcal{R}}\right|^2\mathrm{d}\lambda\,\mathrm{d}l \tag{42}$$

where the integral with respect to λ is carried out over all rays reaching the far field from a given source location.

$\bar{\mathcal{R}} \equiv 1$ for a hard-walled duct, and

$$\begin{aligned}\bar{I} = &\frac{lk_s^4}{2\left[2\pi R\bar{c}_s\bar{c}_\infty(1-M_s\cos\theta_\infty)(1-M_c\cos\theta_\infty)^2\right]^2} \\ &\times\left\{\frac{[1-M_s\cos\theta_\infty]^4}{(\bar{c}_s/\bar{c}_\infty)^4}\mathcal{Q}_0 + \cos^4\theta_\infty\mathcal{Q}_{11}\right. \\ &\left. + 2q_s^2\cos^2\theta_\infty\mathcal{Q}_{12} + q_s^4\mathcal{Q}_{22}\right\}\end{aligned} \tag{43}$$

at the polar angles for which all rays reach the far field.

This shows that the polar directivity and intensity of the circumferentially averaged sound field then depend only on the local Mach number, sound speed, and source characteristics and are unaffected by the details of the sound propagation through the actual flow. This is also true when the source is downstream of the duct exit, that is, for externally generated noise. This is not, however, true for a soft-walled duct where the detailed three-dimensional propagation effects can significantly influence the circumferentially averaged sound field through the reflection coefficient $\bar{\mathcal{R}}$.

These results suggest that it may be possible to tailor the mean-flow and sound source distribution within the nozzle, for example, by appropriately shaping the mixer lobes, to improve the effectiveness of the acoustic liner, which is one of the main objectives of the mixer–ejector development.

Application to a Rectangular Duct

As indicated in the Introduction, rectangular mixer–ejectors are likely to be the nozzle of choice for the next generation of high-speed aircraft. It is appropriate to model the nozzle geometry by superelliptical cross sections:

$$\chi(x_2, x_3) = (x_2/A)^r + x_3^r \tag{44}$$

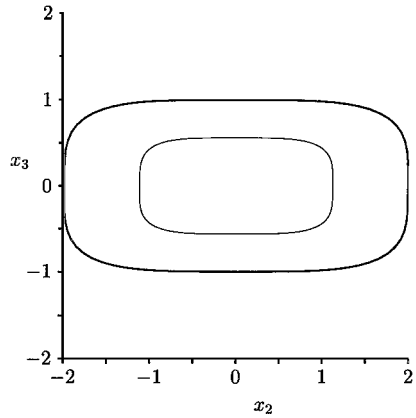

Fig. 3 Superellipse geometry; $A = 2$ and $r = 4$.

This functional form yields an elliptical shape when $r = 2$ and approaches a rectangle as $r \to \infty$. The duct surface resembles a rectangle with rounded corners at intermediate values of r. The duct cross section and source distribution for an aspect ratio of two with $r = 4$ and $\chi_s = 0.1$ are shown in Fig. 3.

Numerical Procedure

Calculation of the far-field sound spectral density requires the numerical solution of the ray equations (10–12) to obtain the ray-spreading factors and reflection coefficients that appear in the relevant formulas.

An iterative procedure was used to find the rays reaching a given observer location from each source location on the ring (37) in computations for the azimuthal variation of the far-field spectral density. Starting conditions were generated from solutions to the ray equations for a given set of initial ray directions, λ, for each source location and far-field polar angle. Results from this first stage of the computation were also used to evaluate the polar variation of the circumferentially averaged sound. These calculations are significantly impacted by the reduction of the ray computations to two dimensions.

The ray-spreading factor was computed by solving the evolution equations for $\partial \boldsymbol{x}_t / \partial \lambda$ simultaneously with the basic ray equations (for example, see Candel[13]). The reflection coefficient was computed by keeping track of the incident normal component of $\boldsymbol{s}$ at each wall reflection [see Eqs. (15–17)]. Once the trajectories of the rays reaching the desired far-field azimuthal locations have been found, they are saved and can be used in computations for other cases with the same ray paths. In particular, results for different normalized wall impedance values can be quickly obtained in this way.

A large number of ray trajectories must be computed to map completely the sound field. However, because each trajectory is completely independent of all of the others, the application of parallel processing techniques can produce dramatic reductions in computational time. The present numerical results were computed on a cluster of eight personal computers using the Message Passing Interface.[14,15]

The required ray calculations are divided as equally as possible among the available processors in the first-stage ray computations. To calculate the azimuthal sound variation, each processor is assigned a set of source locations on the ring (37). It then determines the rays (and associated ray-spreading factors and reflection coefficients) reaching the desired azimuthal locations from those source locations and evaluates the relevant portion of the integral in Eq. (40). The pieces of the integral are then collected and summed to obtain the final result. The symmetry of the problem is used to reduce the source locations that need to be considered to those located in the first quadrant of the (x_2, x_3) plane.

For each ring source, typical runs for the azimuthal sound variation at a given far-field polar angle take about 1 h of computational time per processor on a cluster of eight Pentium III-based workstations, once the ray starting conditions are obtained. The highly parallel nature of the calculations, however, suggests that efficient use could be made of massively parallel computer systems consisting of hundreds (or even thousands) of processors.

Results

Numerical results were obtained for a uniform sound speed and the mean Mach number profile

$$M(\boldsymbol{x}_t) = M_0 \frac{\left(\exp\left\{-a\left[x_3^r + (x_2/A)^r\right]^b\right\} - \exp(-a)\right)^n}{[1 - \exp(-a)^n]} \tag{45}$$

where M_0 is the centerline Mach number and the parameters a, b, and n are used to control the profile shape. $M(\boldsymbol{x}_t)$ goes to zero at the duct wall and is assumed to remain zero beyond that point.

The relative contributions of the source terms in Eqs. (38) and (43) were determined by using the axisymmetric turbulence source model functions proposed by Khavaran.[16] The anisotropy in this model is characterized by the two parameters u_2^2/u_1^2 and L_2/L_1, where u_1^2 and u_2^2 are the streamwise and transverse mean-square turbulent velocities, respectively, and L_1 and L_2 are the corresponding correlation lengths.[16] Values of $u_2^2/u_1^2 = 0.6$ and $L_2/L_1 = 0.5$ were used in the calculations.

We begin by presenting results for parameter values typical of some recent rectangular mixer–ejector tests and then proceed to show how varying some of these parameters affects the sound field.

Figure 4a shows the polar variation of the azimuthally averaged sound field for a duct of aspect ratio 1.5 and $M_0 = 0.9$. Results are shown for hard- and soft-walled ducts with normalized wall impedance values (indicated in Fig. 4 caption) typical of those used in the nozzle tests. For comparison, Fig. 4b shows the corresponding results for a circular duct. The polar directivity of the azimuthally averaged sound field for a hard-walled duct was shown to be independent of ray propagation effects. The polar directivity for the

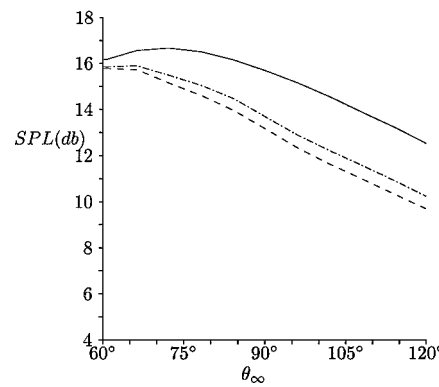

a) Superellipse with $A = 1.5$

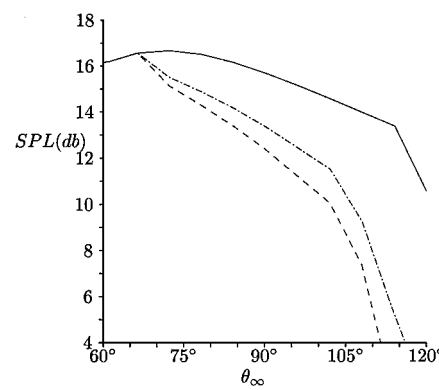

b) Circular duct

Fig. 4 Polar variation of the azimuthally averaged sound pressure level at constant source frequency due to a ring source at $x_1^s = -0.5$, $\chi_s = 0.1$. The Mach number profile parameters are $M_0 = 0.9$, $a = 2$, $b = 2$, $n = 8$; ——, hard wall; – – –, $\zeta = (1, 1)$; and –·–, $\zeta = (2, 2)$.

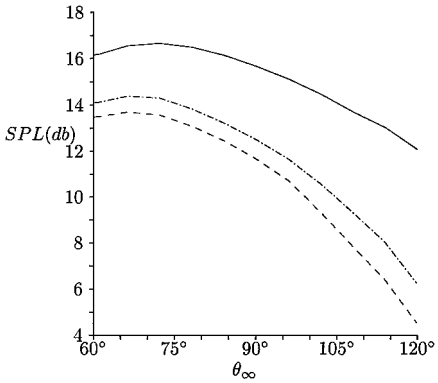

a) Superellipse with $A = 1.5$

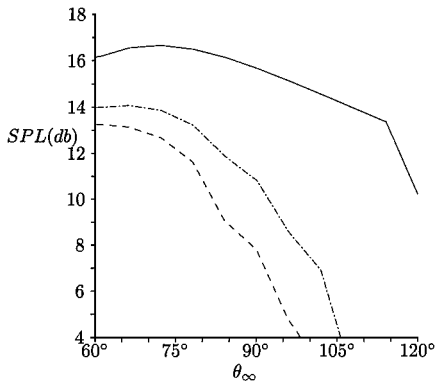

b) Circular duct

Fig. 5 Polar variation of the azimuthally averaged sound pressure level at constant source frequency due to a ring source at $x_1^s = -1.0$, $\chi_s = 0.1$. The Mach number profile parameters are $M_0 = 0.9$, $a = 2$, $b = 2$, $n = 8$; ——, hard wall; – – –, $\zeta = (1, 1)$; and –·–, $\zeta = (2, 2)$.

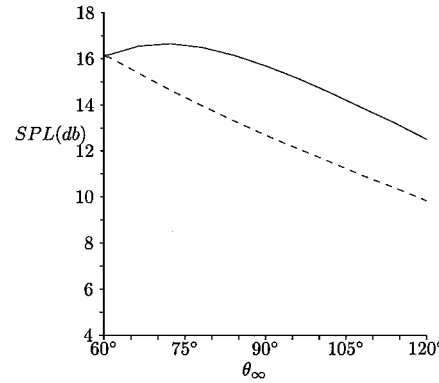

Fig. 6 Comparison of the polar variation of the azimuthally averaged sound pressure level at constant source frequency for a superelliptical duct with $A = 1.5$ obtained using an axisymmetric (——) and isotropic (– – –) description of the turbulence for the source term. Source location is $x_1^s = -0.5$, $\chi_s = 0.1$.

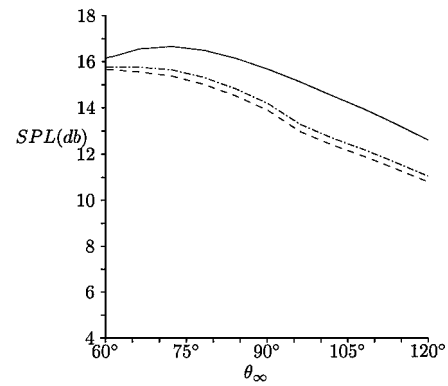

Fig. 7 Polar variation of the azimuthally averaged sound pressure level at constant source frequency for a superelliptical duct with $A = 4.0$ due to a ring source at $x_1^s = -0.5$, $\chi_s = 0.1$. Mach number profile parameters are $M_0 = 0.9$, $a = 2$, $b = 2$, $n = 8$; ——, hard wall; – – –, $\zeta = (1, 1)$; and –·–, $\zeta = (2, 2)$.

superellipse and round duct are, therefore, the same at the polar angles where all rays reach the far field. Figure 4 shows that rays begin to be cut off at smaller angles to the jet axis (but still in the upstream quadrant) for the circular duct. On the other hand, the polar directivity for an acoustically treated duct can be significantly influenced by these effects because the wall reflections are influenced by the propagation of the sound through the mean flow as well by as the duct geometry. Sound suppression (about 2 dB) with the superelliptic duct is comparable with that of the circular duct at polar angles near the peak of the directivity curve, but the wall impedance has a greater effect in the circular duct as θ_∞ increases, especially in the upstream quadrant.

The streamwise location of the dominant internal sound sources is an important factor in determining the effectiveness of the acoustic liners. Figure 5 shows the effect of the axial source location on the azimuthally averaged polar directivity. As expected, the acoustically treated walls absorb more sound when the source lies farther upstream from the duct exit because the rays then undergo more reflections. The additional wall reflections also cause a larger variation in the sound pressure levels when the wall impedance is varied.

The azimuthal directivity of the sound field at a given far-field polar angle was shown to be unaffected by the weighting of the various quadrupole components. Equation (43) however, clearly shows that the polar variation is influenced by this weighting. Figure 6 compares the polar variation of the azimuthally averaged sound field for the case shown in Fig. 4 with the corresponding result for isotropic turbulence. The polar variation is given by two inverse Doppler factors in the isotropic case, and the sound pressure level drops off more rapidly with angle from the jet axis than for the axisymmetric case.

Figure 7 shows the azimuthally averaged polar directivity for a duct of aspect ratio four. The acoustic liner produces slightly less suppression than in the smaller aspect ratio duct on an azimuthally averaged basis.

Figure 8 shows the azimuthal variation of the sound spectra at a number of far-field polar angles for a duct of aspect ratio 1.5. There is a large azimuthal variation of the sound pressure level at the smallest polar angle (outside the zone of silence) to the jet axis ($\theta_\infty = 60$ deg), with a sharp drop at angles near the duct corners. The sound pressure level becomes more uniform azimuthally as θ_∞ increases toward 90 deg but again exhibits a substantial azimuthal variation when θ_∞ is further increased into the upstream quadrant.

The acoustic liners have very little effect on the sound radiated at $\theta_\infty = 60$ deg (see also Fig. 4). The little suppression that does occur at this angle is concentrated above and at the sides of the duct. Most rays undergo just one wall reflection in this case, and some do not encounter the wall at all. The reduction is fairly uniform circumferentially at larger angles from the jet axis.

Figure 9 shows corresponding results for a case where the source is located farther upstream in the duct. There is now less azimuthal variation at the smaller angles to the jet axis in the hard-wall case than in the preceding results, possibly because a second wall reflection that occurs for certain rays from this source location causes some of the rays to reach nearly the same far-field azimuthal location as they would in the absence of the wall. However, the additional wall reflections also cause the wall impedance to have a more significant effect on the far-field sound, and there is now much greater sound suppression in the corner directions for $\theta_\infty = 60$ and 70 deg. The wall liner is very effective in suppressing the sound in the upstream quadrant in this case.

Figure 10 shows the variation in the azimuthal sound pressure level for a hard-walled duct of aspect ratio 4. The variation is larger

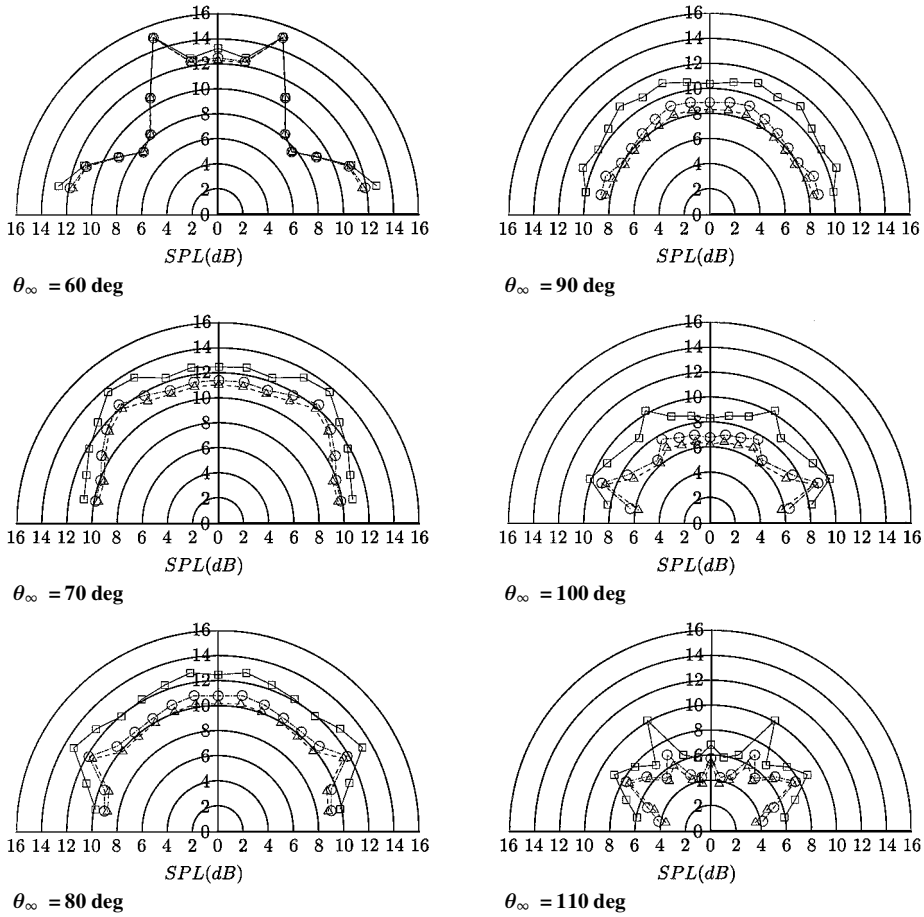

Fig. 8 Azimuthal variation of the sound pressure level at constant source frequency from a ring source at $x_1^s = -0.5$, $\chi_s = 0.1$ within a superelliptical duct with $A = 1.5$, for various far-field polar angles and wall impedances; □, hard wall; △, $\zeta = (1, 1)$; and ○, $\zeta = (2, 2)$.

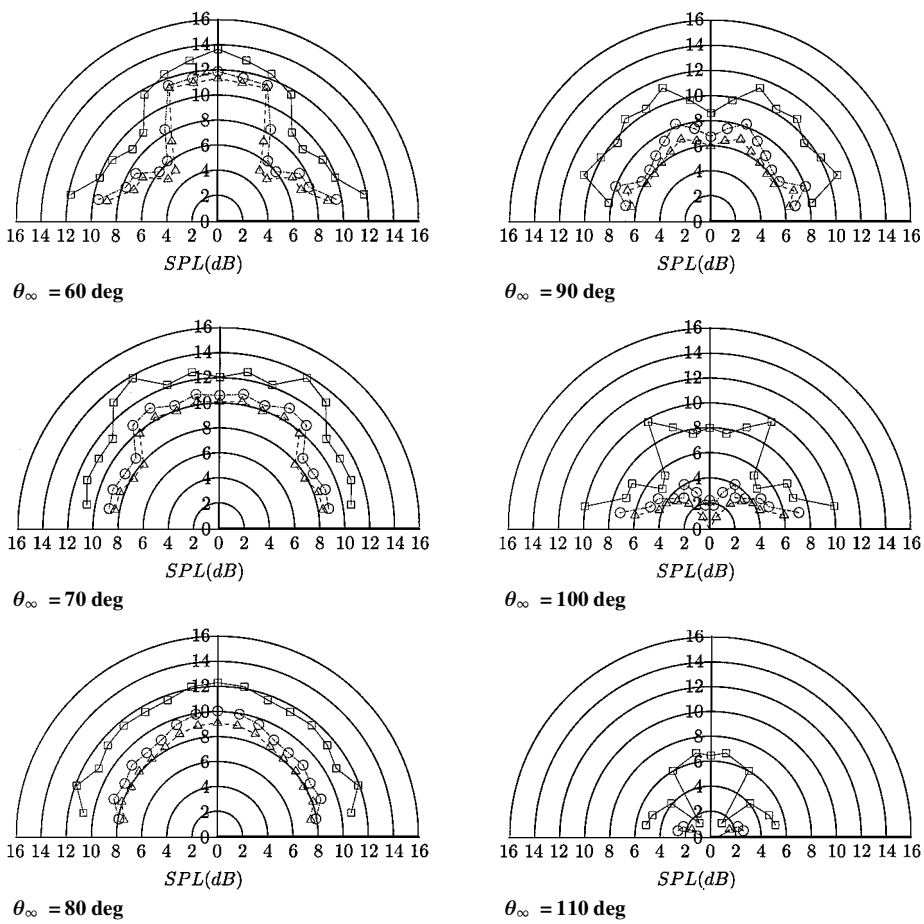

Fig. 9 Azimuthal variation of the sound pressure level at constant source frequency from a ring source at $x_1^s = -1.0$, $\chi_s = 0.1$ within a superelliptical duct with $A = 1.5$, for various far-field polar angles and wall impedances; □, hard wall; △, $\zeta = (1, 1)$; and ○, $\zeta = (2, 2)$.

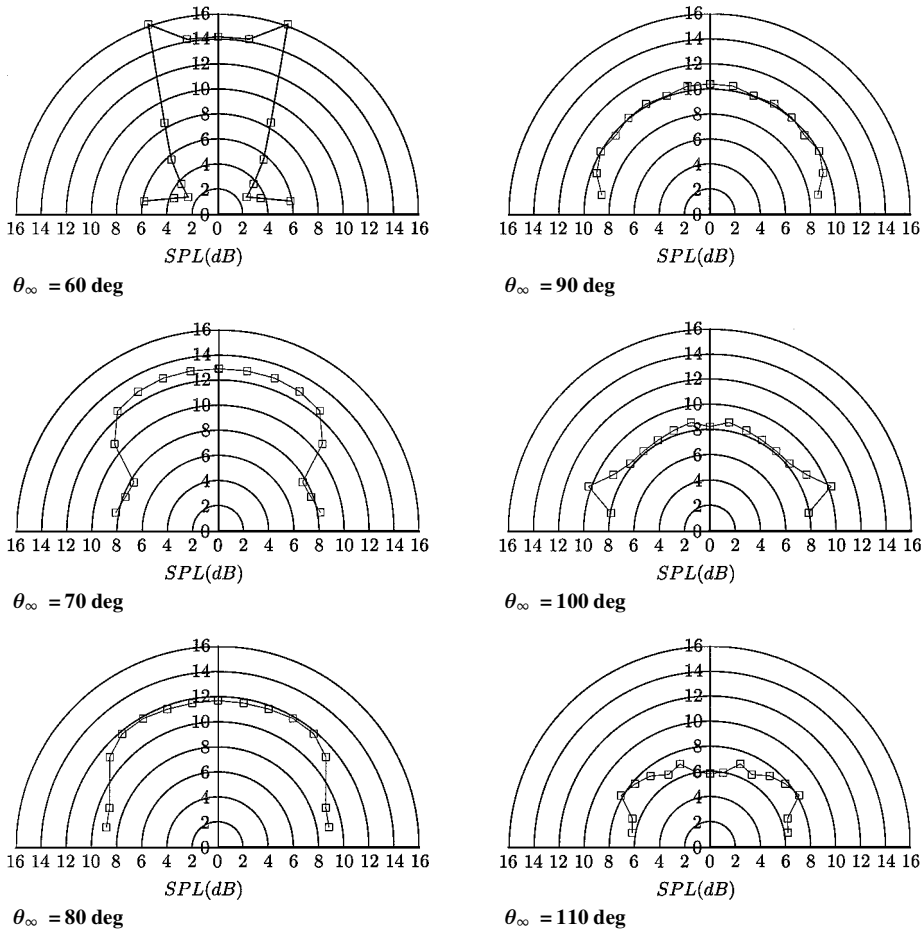

Fig. 10 Azimuthal variation of the sound pressure level at constant source frequency from a ring source at $x_1^s = -0.5$, $\chi_s = 0.1$ within a superelliptical duct with $A = 4.0$, for various far-field polar angles.

at polar angles in the downstream quadrant for the higher-aspect-ratio duct.

Conclusions

A previously derived high-frequency solution to Lilley's equation[5] is used to study the far-field characteristics of the sound generated by a turbulent flow within a nonaxisymmetric nozzle. The turbulence is assumed to be axisymmetric about the mean-flow direction to simplify the source terms. A relatively simple formula for the far-field azimuthal and polar sound field variation is obtained when the source distribution is represented by a concentrated ring concentric with the duct walls, and the mean-flow and turbulence statistics are assumed to be uniform along the source distribution. The numerical computations require the calculation of multiple ray trajectories, and the paper has described the development of an efficient computer code for parallel computation of these rays. The code is suitable for use on large, massively parallel, computer systems, and preliminary runs on an ORIGIN 2000 system with 512 processors show that results for the azimuthal directivity patterns can obtained in a few minutes of wall-clock time. However, it is also quite feasible to run the code on much smaller (and cheaper) clusters of workstations.

The method has been applied to the case of a rectangular duct, which is a geometry under consideration for use on the next generation of high-speed aircraft. Results for the azimuthal and polar variation of the sound field for a duct aspect ratio and wall impedances relevant to recent prototype tests have been presented. Results for a number of other cases were also presented to demonstrate the utility of the procedure.

Future plans include carrying out timing studies to quantify the expected computational gains with increasing numbers of processors and making quantitative comparisons of predicted results with recent experimental data.

Acknowledgments

The authors would like to thank James Bridges of NASA John H. Glenn Research Center at Lewis Field for information about the geometry and flow conditions relevant to the mixer-ejector tests, and Mary Jo Long-Davis of NASA Glenn for providing support for computer time on the NAS ORIGIN 2000 systems at NASA Ames Research Center.

References

[1] Goldstein, M. E., and Rosenbaum, B. M., "Emission of Sound from Turbulence Convected by a Parallel Flow in the Presence of Solid Boundaries," NASA TN D-7118, Oct. 1973.

[2] Dill, L. H., Oyediran, A. A., and Krejsa, E. A., "Refraction of Sound Emitted Near Solid Boundaries from a Sheared Jet," NASA TM 1998-207421, May 1998.

[3] Goldstein, M. E., "High Frequency Sound Emission from Moving Point Multipole Sources Embedded in Arbitrary Transversely Sheared Mean Flows," *Journal of Sound and Vibration*, Vol. 80, No. 4, 1982, pp. 499–522.

[4] Durbin, P. A., "High Frequency Green Function for Aerodynamic Noise in Moving Media, Part I: General Theory," *Journal of Sound and Vibration*, Vol. 91, No. 4, 1983, pp. 519–525.

[5] Goldstein, M. E., and Leib, S. J., "Emission of Sound from Turbulence Convected by a Parallel Mean Flow in the Presence of a Confining Duct," *Journal of Sound and Vibration*, Vol. 235, No. 1, 2000, pp. 25–42.

[6] Kempton, A. J., "A Ray-Theory Approach for High-Frequency Engine-Intake Noise," *Mechanics of Sound Generation in Flows*, Springer-Verlag, Berlin, 1979, pp. 203–209.

[7] Goldstein, M. E., *Aeroacoustics*, McGraw–Hill, New York, 1976, pp. 2–10.

[8] Ffowcs Williams, J. E., "The Noise from Turbulence Convected at High Speed," *Philosophical Transactions of the Royal Society, Series A: Mathematical and Physical Sciences*, Vol. A255, April 1963, pp. 469–503.

[9] Goldstein, M. E., and Rosenbaum, B. M., "Effect of Anisotropic Turbulence on Aerodynamic Noise," *Journal of the Acoustical Society of America*, Vol. 54, No. 3, 1973, pp. 630–645.

[10]Durbin, P. A., "High Frequency Green Function for Aerodynamic Noise in Moving Media, Part II: Noise from a Spreading Jet," *Journal of Sound and Vibration*, Vol. 91, No. 4, 1983, pp. 527–538.

[11]Millionschikov, M. D., "Theory of Homogeneous Isotropic Turbulence," *Doklady Akademii Nauk SSSR*, Vol. 32, No. 9, 1941, pp. 611–614.

[12]Batchelor, G. K., *Theory of Homogeneous Turbulence*, Cambridge Univ. Press, Cambridge, England, U.K., 1953, p. 179.

[13]Candel, S. M., "Numerical Solution of Conservation Equations Arising in Linear Wave Theory: Application to Aeroacoustics," *Journal of Fluid Mechanics*, Vol. 83, Pt. 3, 1977, pp. 465–493.

[14]Gropp, W., Lusk, E., Doss, N., and Skjellum, A., "A High-Performance Portable Implementation of the MPI Message Passing Interface Standard," *Parallel Computing*, Vol. 22, No. 6, 1996, pp. 789–828.

[15]Gropp, W. D., and Lusk, E., "User's Guide for mpich a Portable Implementation of MPI," Argonne National Lab., Rept. ANL-96/6, Argonne, IL, 1996.

[16]Khavaran, A., "Role of Anisotropy in Turbulent Mixing Noise," *AIAA Journal*, Vol. 37, No. 7, 1999, pp. 832–841.

W. J. Devenport
Associate Editor